Effect of lateral confinement on valence-band mixing and polarization anisotropy in quantum wires

F. Vouilloz, D. Y. Oberli, M.-A. Dupertuis, A. Gustafsson, F. Reinhardt, and E. Kapon
Département de Physique, Ecole Polytechnique Fédérale de Lausanne, CH-1015 Lausanne, Switzerland
(Received 31 July 1997; revised manuscript received 1 December 1997)

The optical properties of high-quality V-groove GaAs/$Al_xGa_{1-x}As$ quantum wires have been investigated using low-temperature photoluminescence (PL) and photoluminescence excitation (PLE) techniques. We systematically study the evolution of PL and PLE spectra as a function of the wire size. This comparison allows us to analyze the modification of one-dimensional subbands with decreasing wire thickness. We clarify the influence of surface corrugation and localization effects on PL and PLE spectra and we observe large polarization anisotropy unambiguously related to the one-dimensional character of our quantum wires. The results of a polarization analysis of the excitonic transitions are combined with a calculation of the electronic band structure to identify the nature of the transitions and the impact of two-dimensional quantum confinement on valence-band mixing. The observed large polarization anisotropy is directly compared to the effects predicted by a four-band $\mathbf{k}\cdot\mathbf{p}$ model calculation of the valence-band structure. The set of experimental results combined with our model calculations is consistent with a strong suppression of band-edge absorption in these one-dimensional structures. [S0163-1829(98)08319-2]

I. INTRODUCTION

The electronic band structure and the optical properties of low-dimensional systems, particularly semiconductor quantum wires (QWRs) and quantum dots, have been attracting considerable interest recently.[1] The lateral quantum confinement and reduced dimensionality in these artificial structures can be employed to tailor their electronic and optical properties so as to allow the realization of band structures not achievable in bulk materials. The resulting structured materials may find important applications in novel electronic and optical devices, especially since the quantum confinement and low dimensionality lead to enhancement of the density of states at specific energies. Furthermore, modification in the electron-hole Coulomb interaction in these structures increases the importance of excitonic effects.[2,3] These features could allow the utilization of the more confined character of the electronic states in low-dimensional systems, particularly useful in optical applications, together with the delocalized nature of the states in bulk semiconductors, widely employed in devices relying on carrier transport.

The band structure of one-dimensional (1D) semiconductor QWRs has been extensively investigated theoretically using model systems.[4,5] Whereas theoretical models of the 1D conduction band predict effects largely similar to that in 2D quantum wells (QWs), i.e., quantization of subbands due to quantum confinement, studies of the nature of the valence-band states have revealed features unique to 1D systems. Unlike the case of QWs, the quantum confinement in two spatial directions gives rise to valence-band mixing at the *center* of the Brillouin zone. The mixing of the heavy hole (hh) and light hole (lh) states, which can be tuned by the lateral confinement potential, leads to modified energies of the optical interband transitions and to a redistribution of the oscillator strength. Moreover, the modified valence-band structure results in intrinsic polarization anisotropy of the interband absorption spectra, whose nature is intimately related to the details of the band mixing in the 1D system.[6]

We have reported recently a combined experimental and theoretical study of the optical properties of high-quality 1D semiconductor QWRs and have shown that the observed optical anisotropy in the linearly polarized excitation spectra of these wires arises solely from the 1D nature of the electronic band structure.[6] The purpose of this paper is to present a systematic investigation of the effect of lateral confinement on photoluminescence (PL) and photoluminescence excitation (PLE) spectra of GaAs/$Al_xGa_{1-x}As$ QWRs. Owing to the nonmonotonous evolution of the optical properties with changing wire thickness this requires the simultaneous experimental study of QWRs of various sizes and theoretical calculations of the corresponding band structures and optical transitions. Moreover, we will show that *localization effects strongly influence the polarization anisotropy of PL spectra and prevent therefore any polarization analysis based on extended states*.

Up to now the experimental study of the band structure of 1D systems has been hampered by the technological challenge in producing QWRs with sufficiently small inhomogeneous broadening. The effect of lateral quantum confinement on the conduction band has been evidenced by the emergence of 1D subbands in the optical luminescence characteristics of QWR structures prepared by different approaches.[7–10] However, the observation of the details of the valence-band structure requires the resolution and identification of several 1D valence-band states. Furthermore, the use of optical anisotropy as a probe of the valence-band mixing prerequires the identification and separation of other physical effects,[11] particularly strain,[12,13] electromagnetic effects due to surface corrugations,[14] and intrinsic bulk valence-band anisotropy,[15] which can screen the intrinsic 1D effects. Specific morphologies of a quantum well interface which contains partially ordered and elongated monolayer islands are also known to be a source of optical anisotropies

unrelated to any lateral confinement.[16] Indeed, attempts to observe the intrinsic polarization anisotropy in several types of QWR structures could not unveil the intrinsic 1D valence-band structure because of these spurious effects.[12,17–19] Among the experimental studies, Bloch, Bockelmann, and Laruelle[20] and more recently Goldoni *et al.*[21] obtained information about the valence subbands of their QWR structures from anisotropy spectra but could not directly relate them to the observation of 1D excitonic transitions. Akiyama, Someya, and Sakaki[22] have observed optical anisotropy induced by lateral confinement in T-shaped QWRs but the overlap of photoluminescence excitation peaks with other spectral features hindered observation of excited 1D states.

On the contrary, the high quality of our QWRs results in clear observation of excitonic transitions between 1D quantum-confined energy levels. This enables us to study in detail the impact of two-dimensional quantum confinement on valence-band mixing and polarization anisotropy of PL and PLE spectra. Our systematic studies provide further insight into the relationship between the optical polarization anisotropy and the valence-band structure of 1D semiconductors. The outline of the paper is the following. In the experimental part (Sec. II) we describe the QWR structures (Sec. II A) and the experimental techniques used (Sec. II B). In Sec. III we summarize the essential features of a four-band $\mathbf{k}\cdot\mathbf{p}$ model of the band structure, fully taking into account the geometry of the actual QWR structures. Section IV, which describes the experimental results, is divided into two parts. In Sec. IV A we present PL spectra and we show the influence of localization effects on their polarization properties. In Sec. IV B we present linearly and circularly polarized PLE spectra and we discuss polarization effects related to exciton localization and surface corrugation. In Sec. V we use the results of the model, namely, subband spacings and optical matrix elements, to analyze and discuss the experimental linearly and circularly polarized PLE spectra. Finally, in Sec. VI we summarize our results and conclude.

II. EXPERIMENT

A. Structure

GaAs QWRs embedded in $Al_{0.3}Ga_{0.7}As$ were grown by low-pressure organometallic chemical vapor deposition (OMCVD) on grooved (001)-GaAs substrates ($\pm 0.1°$), with the wires oriented in the $[1\bar{1}0]$ direction.[23] The periodic corrugations were made by holographic photolithography and wet chemical etching. The growth of the structures was carried out in a horizontal reactor with a rotating susceptor plate. The partial pressures of the growth species were 0.159 μbar for trimethylaluminum, 1.52 μbar for trimethylgallium, and 0.33 μbar for arsine. H_2 was used as the carrier gas at a total pressure of 20 mbar and a flux of 6 l/min, resulting in a nominal [(100) planar] growth rate of 0.38 and 0.25 nm/s for $Al_xGa_{1-x}As$ and GaAs, respectively. The substrate temperature was 680 °C.

We have studied three samples, each consisting of a 0.5 μm pitch lateral array of single QWRs of different sizes. The nominal GaAs layer thicknesses were 5 nm, 2.5 nm, and 1.5 nm, resulting in a thickness at the crescent center of 14.1 nm, 8.8 nm, and 4.1 nm, respectively. A sufficiently thick $Al_xGa_{1-x}As$ cladding layer was grown on top of the QWR array in order to eliminate the surface corrugation and reduce drastically electromagnetic effects (grating coupler,[17] local field[4]) that might contribute to the optical anisotropy of the samples.[17,18,24,25]

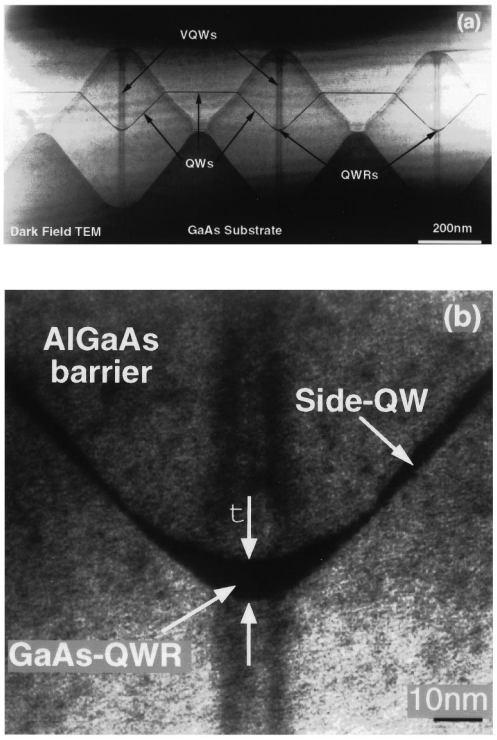

FIG. 1. TEM micrograph showing a cross-sectional view of (a) a part of a QWR array on a 0.5 μm pitch grating, and (b) the QWR region. The nominal GaAs thickness is 2.5 nm, and the resulting GaAs crescent is 8.8 nm thick at its center.

A typical cross-sectional view of the QWR heterostructure is shown in the transmission electron microscope (TEM) micrograph of Fig. 1. At the bottom of the grooves, crescent-shaped QWRs are produced due to the combined effects of groove sharpening during $Al_xGa_{1-x}As$ growth and the higher growth rate of GaAs.[7] The QWR regions are connected to side-QW structures via a constriction. Note also the vertical dark stripe running through the QWRs; this Ga-rich region constitutes a vertical $Al_xGa_{1-x}As$ QW (VQW) region which plays an important role in carrier capture into the wires.[26–29]

B. Experimental setup

The samples were mounted in a helium-flow cryostat and kept at 8 K unless it is specified otherwise. The optical spectra were obtained in a pseudobackscattering geometry from the (001) plane using polarized light from an argon-ion laser (488 nm) for the PL measurements and from a tunable titanium-sapphire laser for the PLE experiments. The excitation light was focused into a spot approximately 35 μm in diameter; typical power densities of 25 W/cm^2 were used. The emitted light was dispersed through a Spex-1404 double grating spectrometer and detected with a cooled GaAs photomultiplier using photon-counting mode. For linear polarization measurements, perpendicular (parallel) refers to the

TABLE I. Material parameters of $Al_xGa_{1-x}As$ used in the calculations.

Symbol	Parameter	Unit	$Al_xGa_{1-x}As$
E_g	energy gap	eV	$1.519+1.247x$
$\Delta E_c/\Delta E_v$	band offsets		68/32
m_e	electron mass	m_0	$0.0665+0.0835x$
γ_1	Luttinger parameter		$6.790-3.000x$
γ_2	Luttinger parameter		$1.924-0.694x$
γ_3	Luttinger parameter		$2.681-1.286x$

[110] ([1$\bar{1}$0]) direction. For circular polarization measurements the helicity of the exciting light (σ^+) was fixed. The helicity of the luminescence was analyzed by combining a quarter-wave plate and a linear polarizer in order to transmit the σ^+ or the σ^- component. The spectral resolution was fixed at 4 Å.

C. Theoretical model

For a quantitative understanding of the optical spectra we performed calculations of the confinement energies and squared optical matrix elements for a 2D finite potential-well model. In the following, x is assumed to be along the wire axis, y is the lateral-confinement direction, and z is the growth direction. We solved the 2D Schrödinger equation in the single-particle approximation using effective-mass Hamiltonians for conduction- and valence-band states and a potential profile $V_{e/h}(y,z)$ extracted from the TEM micrograph of the samples. The depth of $V_{e/h}(y,z)$ is given by the band offsets in $Al_xGa_{1-x}As$. The parameters used in the calculations are listed in Table I.[30] The VQW is described by a square potential profile of fixed lateral width and constant depth.

We assume negligible coupling between Γ_6, Γ_7, and Γ_8 bands. The conduction- and valence-band states are built from these bulk bands in the envelope-function approximation.[31] The conduction-band wave functions are written as

$$\Psi^c_{s_z}(\mathbf{r}) = f^c(\mathbf{r}) u^c_{s_z}(\mathbf{r}),$$

where the $u^c_{s_z}(\mathbf{r})$ are the two spin-degenerate ($s=\frac{1}{2}$, $s_z=\pm\frac{1}{2}$) Bloch functions at the bottom of the Γ_6 bulk band. The valence-band states are written as

$$\Psi^v(\mathbf{r}) = \sum_{J_z} f^v_{J_z}(\mathbf{r}) u^v_{J_z}(\mathbf{r}),$$

where the $u^v_{J_z}(\mathbf{r})$ are the degenerate Bloch functions at the top ot the Γ_8 bulk bands. The sum extends over the J_z quantum number ($J_z=\pm\frac{3}{2}$ for the hh, $J_z=\pm\frac{1}{2}$ for the lh) of the $J=\frac{3}{2}$ quadruplet.

In the conduction band, the envelope functions

$$f^c(\mathbf{r}) = \frac{1}{\sqrt{L_x}} \exp(ik_x x)\,\phi(y,z)$$

are the solutions of the following equation:

$$\left[\frac{\hbar^2}{2}\left(k_x^2 \frac{1}{m^*(y,z)} - \frac{\partial}{\partial y}\frac{1}{m^*(y,z)}\frac{\partial}{\partial y} - \frac{\partial}{\partial z}\frac{1}{m^*(y,z)}\frac{\partial}{\partial z}\right) + V_e(y,z)\right] f^c(\mathbf{r}) = E_e f^c(\mathbf{r}),$$

where L_x is the length of the wire, k_x the carrier wave vector along the wire, and $m^*(y,z)$ the bulk conduction electron effective mass at the bottom of the Γ_6 band.

Because of the fourfold degeneracy of the bulk hh and lh bands, the hole subbands are determined from the effective Hamiltonian made up of the 4×4 $\mathbf{k}\cdot\mathbf{p}$ Luttinger Hamiltonian[32] with the potential $V_h(y,z)$ included along the diagonal. Given the orientation of the wires in the heterostructure, the Hamiltonian is rotated so that the new coordinate system is specified by the wire axis $x\equiv[1\bar{1}0]$, $y\equiv[110]$, and $z\equiv[100]$. The total angular momentum $\mathbf{J}$ is quantized along the growth direction z. The Luttinger Hamiltonian expressed in the basis of the eigenstates of $\mathbf{J}$ ($J=\frac{3}{2}$) and J_z,

$$\left|\frac{3}{2},+\frac{3}{2}\right\rangle, \left|\frac{3}{2},+\frac{1}{2}\right\rangle, \left|\frac{3}{2},-\frac{1}{2}\right\rangle, \left|\frac{3}{2},-\frac{3}{2}\right\rangle,$$

is written as

$$H_{\Gamma_8} = \frac{\hbar^2}{2m_0}\begin{pmatrix} P+Q & -S & R & 0 \\ -S^\dagger & P-Q & 0 & R \\ R^\dagger & 0 & P-Q & S \\ 0 & R^\dagger & S^\dagger & P+Q \end{pmatrix},$$

with

$$P = \gamma_1 k_x^2 - \frac{\partial}{\partial y}\gamma_1\frac{\partial}{\partial y} - \frac{\partial}{\partial z}\gamma_1\frac{\partial}{\partial z} + \frac{2m_0}{\hbar^2}V_h(y,z),$$

$$Q = \gamma_2 k_x^2 - \frac{\partial}{\partial y}\gamma_2\frac{\partial}{\partial y} + 2\frac{\partial}{\partial z}\gamma_2\frac{\partial}{\partial z},$$

$$R = \sqrt{3}\left[\gamma_3 k_x^2 + \frac{\partial}{\partial y}\gamma_3\frac{\partial}{\partial y} + k_x\left(\gamma_2\frac{\partial}{\partial y} + \frac{\partial}{\partial y}\gamma_2\right)\right],$$

$$S = \sqrt{3}\left[k_x\left(\gamma_3\frac{\partial}{\partial z} + \frac{\partial}{\partial z}\gamma_3\right) + \frac{\partial}{\partial z}\gamma_3\frac{\partial}{\partial y} + \frac{\partial}{\partial y}\gamma_3\frac{\partial}{\partial z}\right],$$

where m_0 is the free-electron mass and $\gamma_1,\gamma_2,\gamma_3$ are the Luttinger parameters.[33] The wave-vector components k_y and k_z have been replaced by $-i\partial/\partial y$ and $-i\partial/\partial z$, respectively, and the noncommuting products have been symmetrized. Three peculiarities should be noted. First, the choice of the 45°-rotated axes in the x-y plane reverses the roles of γ_2 and γ_3 in the element R, compared to the standard principal axis orientation. Second, our choice of axes also keeps the Luttinger Hamiltonian real. Third, the substitution of the wave-vector components by differentials of the envelope functions must be made separately in the upper and lower triangles of H_{Γ_8}, giving rise to nonidentical but adjoint real operators on both sides of the diagonal. The Schrödinger equations for electrons and holes are solved by a first order finite elements

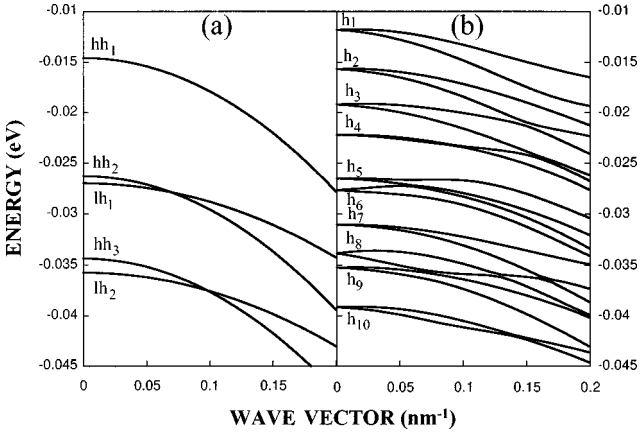

FIG. 2. Valence-band dispersion (a) without and (b) with hh-lh mixing in the 2.5 nm QWR. Subbands in (a) are labeled according to the light or heavy nature of the states at the zone center. Band mixing gives rise to nonparabolic dispersion curves and anticrossing of the subbands; a strong reduction in subband separation is to be noted. Subband splitting away from zone center in (b) is due to the lack of inversion symmetry of the structure.

technique on an irregular mesh made up of quadrilaterals adapted to the actual boundaries of the QWRs.

Figure 2(a) [2(b)] shows the calculated valence-subband dispersion curves for the 2.5 nm QWR without (with) hh-lh mixing. These results demonstrate that band mixing gives rise to nonparabolic dispersion curves and anticrossings of the subbands, a familiar occurrence in the dispersion of QW valence bands. The subband splitting at $k \neq 0$ is due to the lack of inversion symmetry of the structure. Unlike for QWs, the zone-center states for the QWR already contain an admixture of both hh and lh. The percentage lh character of the pair of states at the Γ point is given in Table II for the three QWR samples. The uppermost valence subband is above 90% hh in all three cases whereas the h_6 state of the 5 nm and 2.5 nm QWRs and the h_7 state of the 1.5 nm QWR are above 70% lh at the Γ point (lh-like state).

In the dipole approximation, the absorption coefficient α for a plane electromagnetic wave in a medium of refractive index n is given by

$$\alpha(\omega) = \frac{\pi e^2}{nc\varepsilon_0 m_0^2 \omega V} \sum_{i,f} |\langle f|\hat{\mathbf{e}}\cdot\mathbf{p}|i\rangle|^2 \delta(E_f - E_i - \hbar\omega).$$

TABLE II. Percentage of lh character for valence subbands at the zone center for the (a) 5 nm QWR, (b) 2.5 nm QWR, and (c) 1.5 nm QWR.

					(a)					
Subband	h_1	h_2	h_3	h_4	h_5	h_6	h_7	h_8	h_9	h_{10}
% lh	10	29	43	49	44	70	47	25	49	42
					(b)					
Subband	h_1	h_2	h_3	h_4	h_5	h_6	h_7	h_8	h_9	h_{10}
% lh	10	33	45	53	49	70	46	30	49	45
					(c)					
Subband	h_1	h_2	h_3	h_4	h_5	h_6	h_7	h_8	h_9	h_{10}
% lh	8	22	36	44	46	62	71	52	60	51

ε_0, m_0, V, and $\hbar\omega$ represent the permittivity of vacuum, the free-electron mass, the sample volume, and the photon energy, respectively. In QWRs, this expression yields

$$\alpha(\omega) \propto \sum_{c,v} \int_{\mathrm{BZ}} dk \{|M|^2 \delta(E_c(k) - E_v(k) - \hbar\omega) \times [f_v(E_v(k)) - f_c(E_c(k))]\},$$

where $f_\nu(\varepsilon)$ is the Fermi distribution of carriers in subband ν with a quasi-Fermi level at ε_ν. $|M|^2$ is the squared dipole matrix element of an optical transition between a valence- and a conduction-band state and is written as

$$|M|^2 = \sum_{s_z} \left| \sum_{J_z} \langle f^c(\mathbf{r})|f^v_{J_z}(\mathbf{r})\rangle \langle u^c_{s_z}|\hat{\mathbf{e}}\cdot\mathbf{p}|u^v_{J_z}\rangle \right|^2,$$

where $\hat{\mathbf{e}}$ is the polarization vector of the light and $\mathbf{p}$ is the momentum operator. We define the overlap integrals I_{J_z} as

$$I_{J_z} = \langle f^c(\mathbf{r})|f^v_{J_z}(\mathbf{r})\rangle.$$

The polarization anisotropy of optical transitions measured in PLE experiments is directly related to valence-band mixing[4,5] through the expression of $|M|^2$. Indeed, by developing the preceding relation of $|M|^2$ one can show[4] that the polarization anisotropy of $|M|^2$ in the x-y plane increases in proportion to $(I_{3/2}I_{-1/2} + I_{1/2}I_{-3/2})$ with increasing hh-lh mixing in the valence band.

III. EXPERIMENTAL RESULTS

A. Photoluminescence and its polarization properties

PL spectra for the three QWR samples are displayed in Fig. 3. The different parts of the heterostructure have their distinct luminescence signature. The lowest-energy peak of each spectrum is assigned to the luminescence of the QWR. The broader peak labeled QWs corresponds to that of the side and top QWs. The luminescence from the VQW appears either as a separated peak [Figs. 3(a), 3(b)] or as a shoulder on the high-energy side of QWs' peak [Fig. 3(c)]. Finally, the weaker peak around 1.9 eV is due to recombination in the $Al_xGa_{1-x}As$ barrier material. We found that the integrated QWR luminescence varies linearly with excitation[34] power density between 1 and 10^3 W/cm^2, which supports the intrinsic and excitonic nature of the recombination process.[35] In order to identify the origin of these peaks we have combined a polarization analysis of the luminescence of the heterostructure with a calculation of the confinement energies for the side and top QWs using a finite potential well model. The widths of the QWs were extracted from the TEM micrograph of the sample. The Al concentration at the VQW was determined by cross-sectional atomic force microscopy[36] and was found to be 9% lower than that of the nominal Al value. These peak assignments are supported by low-temperature cross-sectional cathodoluminescence imaging of the emission wavelengths on similar QWR structures.[37]

The PL full width at half maximum (FWHM) of the QWR peak excited with the titanium-sapphire laser ranges from 5.4 to 6.9 meV and the FWHM of the first PLE peak ranges from 3.7 to 12.0 meV for the three samples investigated. The PLE FWHM was determined by fitting the first three PLE peaks

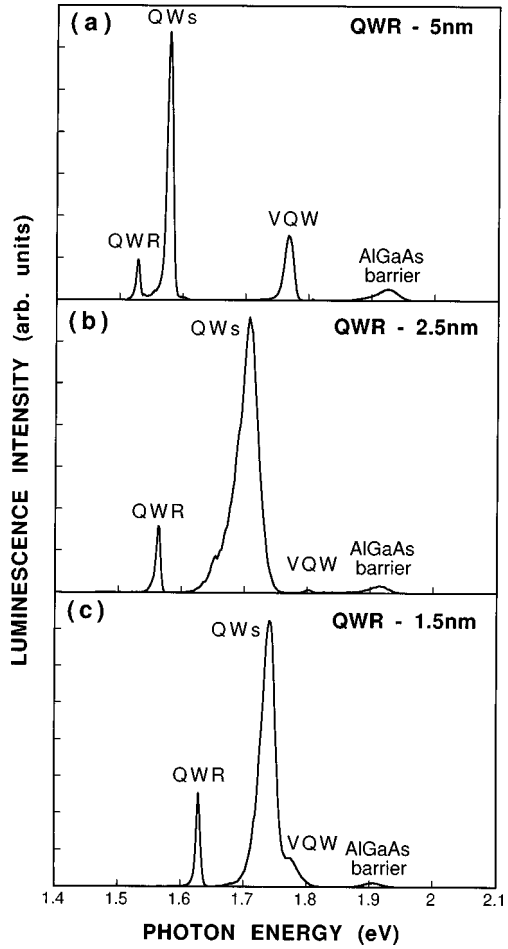

FIG. 3. PL spectra of QWR samples with a nominal GaAs thickness of (a) 5 nm, (b) 2.5 nm, and (c) 1.5 nm, excited with the 488 nm line of an Ar^+ laser ($T=8$ K).

with a superposition of Gaussians. The PLE FWHM is mainly determined by inhomogeneous broadening of an optical transition whereas the PL FWHM strongly depends on relaxation and localization effects. As a consequence, the FWHM of the PLE peaks can be either narrower or broader than that of the corresponding PL peaks.[38] The small Stokes shifts (3.6–8.5 meV) and PLE linewidths attest to the high quality of these wires.

Localization of excitons at interfacial defects can strongly affect the polarization properties of a 2D (Ref. 39) or a 1D system. PL spectra of QW structures which show a fine structure in micro-PL experiments have been assigned by different groups[40–42] to recombination of excitons localized at interface defects caused by roughness or composition fluctuations. We find that the polarization anisotropy of PL spectra is dependent both on excitation wavelength and on the spectral position within the emission line and thus cannot be related to any polarization analysis based on extended states. To illustrate these remarks we show in Fig. 4(a) the PL emission of the 2.5 nm QWR together with its degree of linear polarization $P=(I_{||}-I_{\perp})/(I_{||}+I_{\perp})$, where $I_{||}$ ($I_{\perp}$) is the PL intensity linearly polarized parallel (perpendicular) to the wires. The excitation wavelength was 488 nm. It can be seen that the luminescence is mainly linearly polarized in the wire direction and that P strongly depends on the emission wavelength. The maximum of P is found at a higher energy than

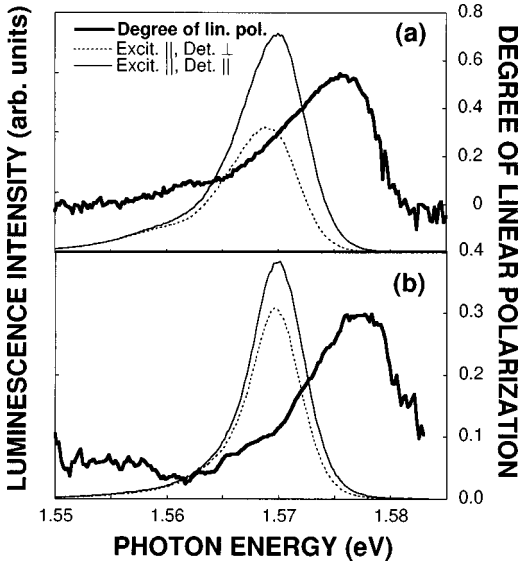

FIG. 4. PL spectra of the 2.5 nm QWR excited by an (a) Ar^+ laser (488 nm) and (b) Ti:sappire laser (710 nm); in both cases the exciting beams were polarized parallel to the wires. The linear polarization of the luminescence was analyzed parallel ($I_{||}$) and perpendicular ($I_{\perp}$) to the wire axis. The degree of linear polarization $P=(I_{||}-I_{\perp})/(I_{||}+I_{\perp})$ is also shown ($T=8$ K).

that of the PL peak for which P is 25%. When the excitation wavelength is increased to 710 nm [Fig. 4(b)] the maximum of P is also blueshifted from the PL peak where P is 11%. This behavior can be attributed to exciton localization due to disorder along the wire. We first note that localized states dominate at the low-energy tail of an inhomogeneous exciton band.[43] Because localization is expected to decrease the degree of linear polarization by symmetrizing the exciton wave function it leads to the lowest degree of linear polarization on the low-energy side of the PL.

B. Photoluminescence excitation and its polarization properties

The linearly polarized PLE spectra of the three QWR samples are shown in Fig. 5(a), Fig. 5(b), and Fig. 5(c), respectively. The dependence of the optical spectra on the polarization of the exciting laser reveals a striking polarization anisotropy. The PLE spectra show up to seven peaks corresponding to excitonic transitions of 1D quantum-confined energy levels. A decrease of the wire thickness leads to a blueshift of the ground-state transition, e_1-h_1, that increases from 1.538 eV for the 5 nm QWR to 1.634 eV for the 1.5 nm QWR. An additional effect which arises from the change in the shape of the crescent for thinner wires leads to a modification of the energy separation between the e_n-h_n transitions. As the crescent thickness decreases, the subband separation first increases, due to the lateral tapering. For thin crescents, however, a further thickness reduction results in a more elongated crescent, which prevents further increase in subband separation. This saturation in the subband separation is enhanced by the increased penetration of the wave function into the surrounding barriers. The separations between the e_1-h_1 and e_2-h_2 transitions are 15.0, 26.5, and 25.3 meV for the 5 nm, 2.5 nm, and 1.5 nm QWR, respectively.

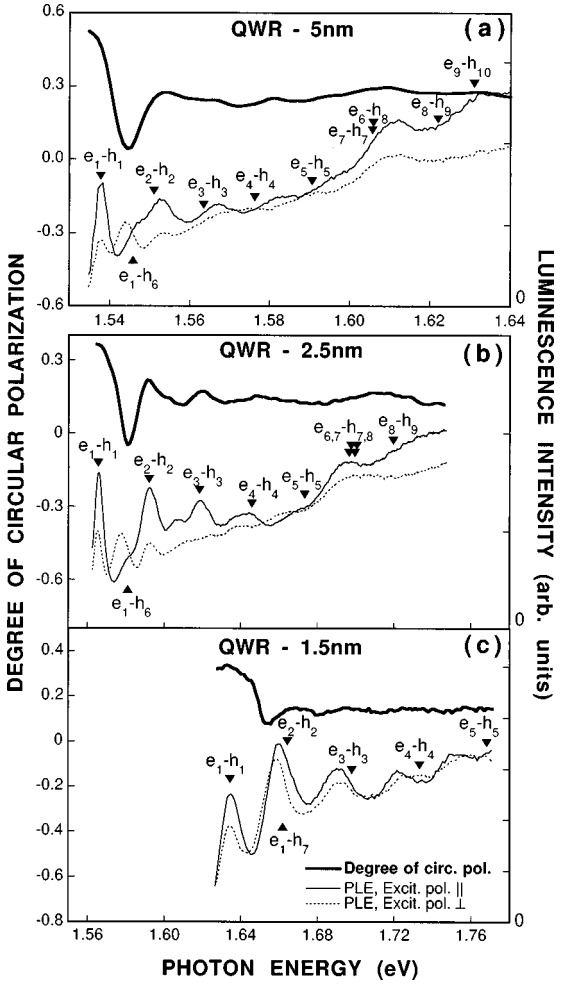

FIG. 5. Degree of circular polarization (see text for definition) and linearly polarized PLE spectra for QWR samples with a nominal GaAs thickness of (a) 5 nm, (b) 2.5 nm, and (c) 1.5 nm. The detection wavelength is set at the maximum of the QWR PL line ($T=8$ K). Note different energy scale for (a).

The presence of corrugations at the surface of a QWR structure causes several electrodynamical effects which may strongly affect the optical properties of the heterostructure. Periodic surface corrugations allow a momentum transfer between photons and the microstructure, giving rise to the so-called grating coupler effect.[44] This leads to a coupling of the photons to nonradiative exciton polaritons in the structured material, which can become observable as an additional strongly polarized signal in the PL spectrum. This effect has been demonstrated in GaAs/Al_xGa_{1-x}As QWs with a modulated cap layer and in etched GaAs/Al_xGa_{1-x}As QWRs for wire widths above 150 nm.[44,45] When the wire width is decreased below 150 nm the QW exciton polaritons localize and a transition to the behavior of quasi-1D excitons is observed.[17] The polarization dependence of the observed optical transitions is then mainly determined by the intrinsic properties of the 1D system.

Corrugations at the surface of a QWR structure also result in local fields characterized by spatial distributions which are polarization dependent.[14] To identify this electrodynamic polarization effect we measured PLE spectra on two different 1.5 nm QWR samples (Fig. 6). The first QWR structure was not planarized and exhibited a periodic modulation of its

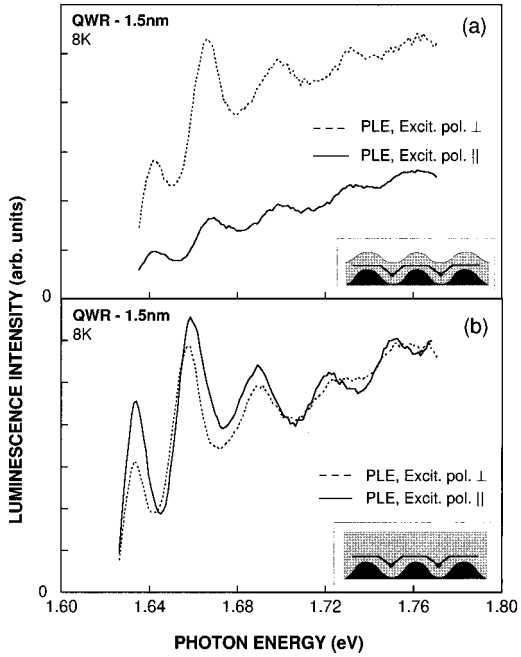

FIG. 6. PLE spectra of 1.5 nm QWRs showing the effect of surface corrugation: (a) 1.5 nm QWR with deep surface corrugation, and (b) 1.5 nm QWR with a planar surface.

surface with grooves approximately 100 nm deep, whereas the second sample was completely planarized. The vertical shift of the PLE spectrum in Fig. 6(a) for excitation light polarized perpendicular to the wires is well explained by the enhancement of the electric field in the grooves of a surface grating when its polarization is orthogonal to the grooves. This, in turn, increases the relative intensities of the PLE lines associated with the QWR transitions for the perpendicular polarization. The polarization dependence of the exciting light intensity at the position of the QWRs thus gives rise to an additional polarization anisotropy modifiying the intrinsic anisotropy of the 1D system.[14]

Figure 6(b) shows PLE spectra of the planarized 1.5 nm QWR. In this case, the same QWR illumination is achieved for the two polarizations. The difference in the luminescence signal for the two different polarizations of the exciting light reflects then the intrinsic properties of the QWRs. We also checked that the PLE spectra and their optical anisotropy did not depend on the incidence angle α of the exciting laser beam, for $\alpha<20°$. For angles $\alpha>20°$ the power reflectance of the incident wave at the surface of the sample critically depends on its polarization state. The PLE spectra presented in Fig. 5 were measured at $\alpha=8.5°$ on planarized structures and are therefore free from surface grating effects.

A PLE spectrum depends both on absorption and emission properties. To investigate the impact of localization effects on the optical anisotropy due to the 1D valence-band structure we measured PLE spectra as a function of the detection wavelength across the PL peak. Figure 7 shows the results for the 1.5 nm QWR. The spectral positions of the different 1D optical transitions do not change notably when the detection wavelength is moved across the PL line. We note, however, that the relative intensity of the first PLE peak with respect to the other peaks decreases as the detection is moved to lower energies. This may indicate that car-

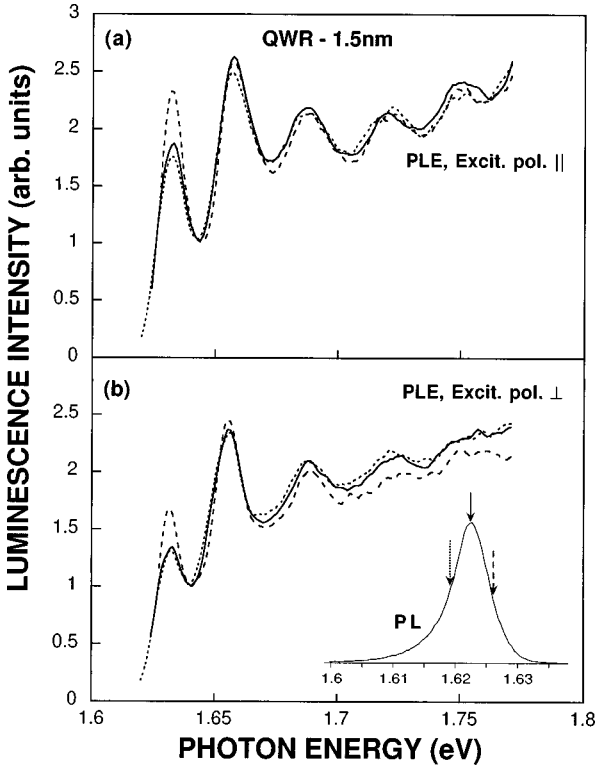

FIG. 7. PLE spectra of the 1.5 nm QWR measured for different detection wavelengths. PLE spectra have been normalized to the local minimum between the two lowest-energy peaks ($T=8$ K).

riers created at the energy of the first PLE peak relax less efficiently when the final state corresponds to strongly localized excitons. Similar results were obtained for the 2.5 nm and 5 nm QWRs. PLE spectra of other comparable QWR samples have been found, nevertheless, to be insensitive to the detection wavelength. In this analysis one should therefore keep in mind that PLE experiments do not exactly reproduce absorption measurements.

Figure 8 shows the ratio of the integrated intensity of the e_1-h_6 transition and that of the e_1-h_1 transition as a function of the angle θ between the polarization direction and the wire axis (2.5 nm QWR). It was determined by fitting the first three PLE peaks with a superposition of three Gaussians. Assuming the squared optical matrix elements $|M|^2_{e_n\text{-}h_m}$ to be constant across each peak, this corresponds to $|M|^2_{e_1\text{-}h_6}/|M|^2_{e_1\text{-}h_1}$. The different curves in Fig. 8 are for PLE spectra detected at different wavelengths across the PL peak. The variation of these polarization anisotropy curves with detection wavelength results from localization effects described previously in this section. Comparison of the data of the 2.5 nm QWR and the 5 nm QWR shows that the maximum ratio (at $\theta=90°$) increases as the overall size of the wire decreases. It should be noted that theoretical calculations in cylindrical QWRs (Ref. 46) yield a vanishing value for light polarized parallel to the wires (at $\theta=0°$), unlike our observation of nonvanishing values in crescent-shaped wires.

To investigate further the nature of the valence states involved in the observed optical transitions, we use circularly polarized light to excite and analyze the QWR luminescence. In this situation the photon helicity is transferred to the semiconductor through spin orientation of the excited electrons

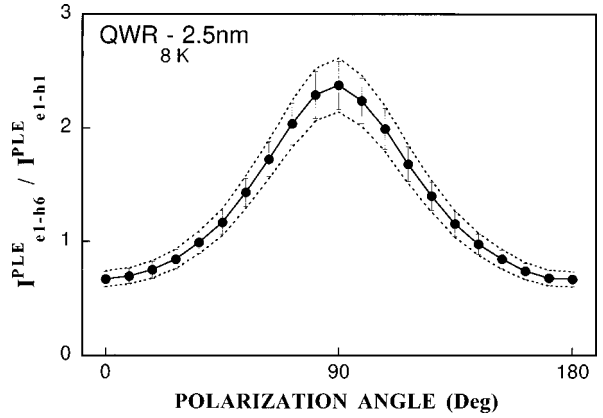

FIG. 8. Ratio of the integrated intensity of the e_1-h_6 transition and that of the e_1-h_1 transition as a function of the angle θ between the polarization direction and the wire axis (2.5 nm QWR). It was determined by fitting the first three PLE peaks with a superposition of Gaussians. The error bars result from the uncertainty of the curve fitting process. The solid line is obtained from PLE spectra detected at the maximum of the QWR PL line, while the upper (lower) dashed line corresponds to low (high) detection energy.

and holes.[48] If we assume incomplete electron spin relaxation;[49] this leads to circular polarization of the PL, which depends on the initial conduction and valence states. The measurement of the degree of circular polarization of luminescence has been used in QWs to identify the hh and lh transitions.[50] In a QWR system light with σ^+ polarization couples hh (lh) component of the wave function with $J_z=-\frac{3}{2}$ $(-\frac{1}{2})$ and electron state with spin $s=-\frac{1}{2}$ $(+\frac{1}{2})$, whereas σ^- polarization couples hh (lh) component of the wave function with $J_z=+\frac{3}{2}$ $(+\frac{1}{2})$ and electron state with $s=+\frac{1}{2}$ $(-\frac{1}{2})$. The measured degree of circular polarization $\mathcal{P}=(I^+-I^-)/(I^++I^-)$, where $I^+(I^-)$ is the $\sigma^+(\sigma^-)$ circularly polarized luminescence intensity, is also shown in Fig. 5 for each QWR structure. The polarization spectra of all three QWRs present strong modulations correlated with the 1D excitonic transitions observed in the linearly polarized PLE spectra. The pronounced dip located at the second lowest-energy transition in each polarization spectrum corresponds to the first valence subband with strong lh character.

IV. DISCUSSION

To analyze the PLE spectral features we implicitly assume a one to one correspondence to absorption peaks as PLE spectra of quantum wells show a close resemblance to calculated absorption spectra.[51] An exact correspondence holds if the relaxation rate from the excited state towards the emitting state dominates over nonradiative recombination rates. We also note that intersubband coupling modifies the overall shape of a PLE spectrum by transferring the oscillator strength towards the low-energy region, which results in a significant increase of the first exciton peak.[3] It is well known that excitonic effects play a major role in the optical-absorption spectra of 2D systems.[47] Moreover, the Sommerfeld factor was calculated[2,3] and found to be much smaller than unity for a direct allowed interband transition in a 1D system, in striking contrast to the 3D and 2D cases. This means that electron-hole correlation leads to a strong sup-

pression of the 1D band-edge singularity in the linear-absorption spectra. For these reasons, we believe that our optical spectra are fully dominated by the excitonic nature of the optical transitions; otherwise, aside from the excitonic peak, a second peak which corresponds to the maximum in the joint density of states (JDOS) would have been observed in the PLE spectra at higher energy. This interpretation of PLE spectra as a single series of peaks for each QWR structure is allowed by the small inhomogeneous broadening of the optical transitions combined with large subband separation and by the comparison with theoretical predictions. We note, however, that band to band transitions may still contribute to the fine structure of the spectra.

In Fig. 5, we indicated the positions of the calculated optical interband transitions. In order to compare the observed 1D excitonic transitions with the calculated interband transitions, we introduced a rigid redshift ($\sim 10-20$ meV) of each series of optical transitions e_n-h_m. The overall agreement with the theoretical calculations is very good for all three investigated samples. Remaining differences may be attributed to slightly different wire cross section in the sample's piece used for the TEM study, to nonparabolicity of the conduction band and additional excitonic effects, which were not included. The binding energy of excitons is indeed expected to vary with the index of the subband[52] but the magnitude of this change is small and believed to be comparable to the difference in binding energies of hh and lh excitons in quantum wells of similar thickness (2 to 3 meV) (Ref. 53) for the two lowest optical transitions.

Optical transitions in Fig. 5 are attributed to QWR states. Comparing PL (Fig. 3) and PLE (Fig. 5) spectra shows that some of these transitions seem to overlap with the states of the 2D QWs. However, carrier transfer from the side QWs into the QWR region is very inefficient at low temperature. This is a consequence of the potential barrier ($\sim$ 40–80 meV) resulting from the necking in the side QWs next to the QWR [see Fig. 1(b)]. We can also exclude the contribution to PLE of absorption and emission from the QW structures since at the spectral position of the QWR emission the intensity of the QW peak is practically negligible (see Fig. 3).

The influence of the lateral confinement in the QWRs on the optical properties manifests itself by a linear-polarization dependence of the PLE spectra. Clear optical anisotropy in absorption is observed for all three samples. The effect is particularly pronounced for the 2.5 nm QWR and for the 5 nm QWR where a distinct crossing in the PLE spectra occurs for the second 1D excitonic transition when measured with orthogonal polarizations. This feature is less pronounced in the PLE spectra of the thinnest 1.5 nm QWR. The weakness of the optical anisotropy in the optical spectra of the 1.5 nm QWR is due to the fortuitous superposition of two optical transitions, e_2-h_2 and e_1-h_7. Within the framework of an adiabatic decoupling of the 2D potential, this occurs when the transverse potential splits the first hh and lh subbands by an amount equal to the energy separating 1D-electron subbands imparted by the lateral potential.[6]

The calculated squared optical matrix elements are displayed in Fig. 9 for all three QWR samples. All the main features of the experimental PLE spectra are remarkably reproduced in Fig. 9: The dominance of the diagonal optical

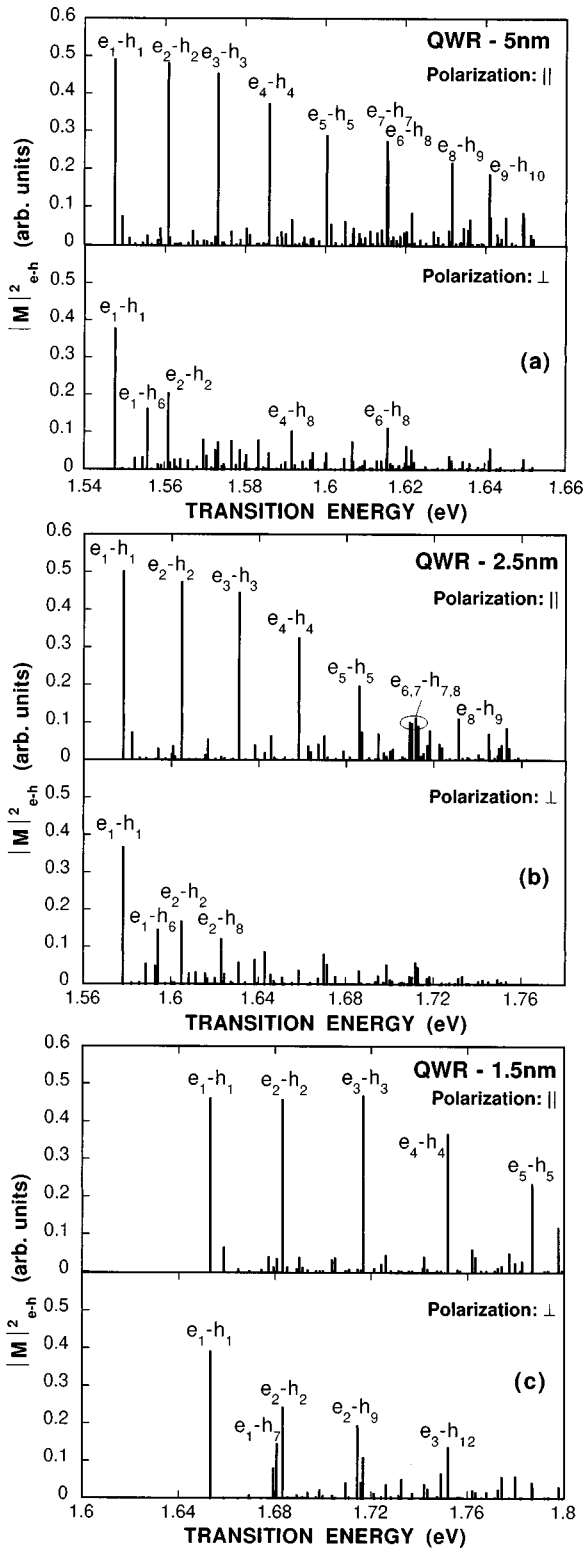

FIG. 9. Square of the optical matrix elements for interband transitions e_i-h_j($1 \leq i,j \leq 10$) calculated at $k=0$ for QWR samples with a nominal thickness of (a) 5 nm, (b) 2.5 nm, and (c) 1.5 nm (no adjustable parameters). Major transitions ($|M|^2_{e\text{-}h} > 0.1$) are labeled according to the indices of the participating electron and hole subbands.

transitions, e_n-h_n, in parallel and perpendicular polarizations is clearly evidenced; in parallel polarization transitions with nonconserving subband indices are strongly suppressed in the low-energy part of the spectra whereas in perpendicular

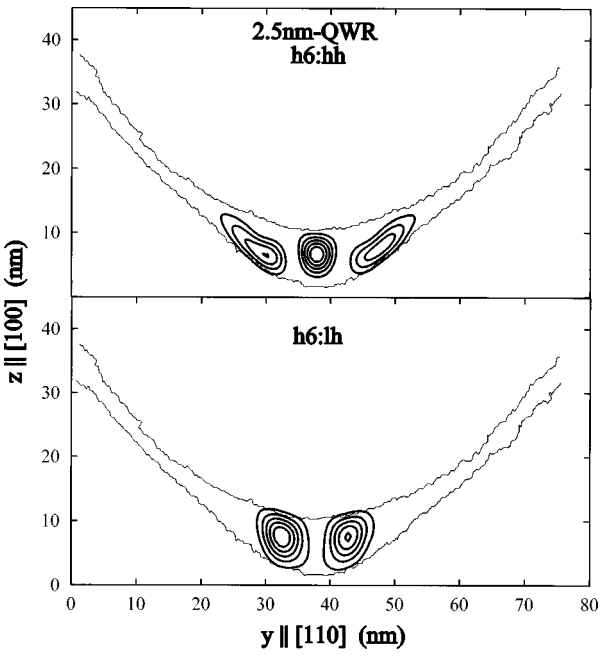

FIG. 10. Confined zone-center hole states in the 2.5 nm QWR structure. The contours of the probability density are plotted for the h_6 state with its constituents of hh and lh. The wire cross section derived from a TEM micrograph and used in the calculation is also shown.

polarization the peaks labeled e_1-h_6 in Figs. 9(a) and 9(b) and e_1-h_7 in Fig. 9(c) carry a significant oscillator strength resulting in a notable polarization anisotropy for the two larger QWRs. This latter feature, clearly visible in Figs. 5(a) and 5(b), originates from the contribution to the valence subband of Bloch states having a dominant lh character.[4,5] Indeed we find a value of 70% lh character for the $n=6$ valence state of the 5 nm and 2.5 nm QWR, and 71% lh character for the $n=7$ valence state of the 1.5 nm QWR (see Table II).

Figure 10 shows the envelope functions of that lh-like *ground state* (h_6) in the 2.5 nm QWR. In fact, two maxima can be observed on the plot of the probability density of its lh constituent (h_6:lh in Fig. 10) because the mixing with higher order states results in a negative interference at the center. The ground-state character is further confirmed by the fact that the two lobes oscillate *in phase* with each other. This state mainly couples to the $n=1$ conduction subband due to a large overlap as can be seen in Fig. 9(b). The wire cross section derived from a TEM micrograph and used in the calculation is also shown in Fig. 10. The fluctuations of the boundaries result from the digitalization of the TEM picture; they have no influence on the calculated wave functions. The e_n-h_m transitions with $n>6$ in Fig. 5(a) and Fig. 5(b) involve transverse electronic states. The corresponding electron wave functions exhibit a node along the growth axis at the center of the QWR and mainly couple to hole states having similar transverse components. As a consequence, major transitions in this spectral region do not necessarily conserve subband indices.[54]

We explain the circularly polarized PLE spectra of the three QWR samples as follows. In the energy range $E_{\mathrm{exc}} < e_1$-''lh''$_1$ only electrons from the lowest valence subbands are excited to the conduction subband e_1. Here ''lh''$_1$ refers to the first valence subband displaying a dominant light hole character. Since the first valence subbands have a dominant hh character (see Table II) the resulting $\mathcal{P}$ is positive, close to 35% at the e_1-h_1 transition in the 1.5 nm and 2.5 nm QWRs and close to 50% in the 5 nm QWR. The deviation from a 100% polarization results on one hand from electron and hole spin relaxation and on the other hand from lh admixture in the h_1 wave function. For an excitation energy approaching the e_1-''lh''$_1$ transition, the electrons originating from the valence subband with strong lh character start to contribute to the luminescence. These electrons are mainly created with $s=+\frac{1}{2}$ and are associated with a negative $\mathcal{P}$ at the e_1-h_1 transition. As the first valence subbands contribute to a positive $\mathcal{P}$, the JDOS for the transition e_1-''lh''$_1$ has to be very high to compensate for it giving rise to a decrease in $\mathcal{P}$. This is further supported by our calculation of the valence-band structure: A negative ''lh'' mass at the center of the Brillouin zone is found in all the QWRs investigated [e.g., see Fig. 2(b)]. This effect explains the pronounced dip located at the e_1-''lh''$_1$ transition in the polarization spectrum of Fig. 5(b). As the excitation energy increases, the JDOS for the e_1-''lh''$_1$ transition falls down and the net polarization increases again. For still higher excitation energies ($E_{\mathrm{exc}} > e_1$-''lh''$_1$) electrons from other valence subbands also appear in the conduction subbands. Because the depolarization increases with the kinetic energy of photocreated electrons,[49] these electrons will only weakly contribute to the polarization and, thus, the circular polarization curve features only small amplitude modulations for optical transitions e_n-h_n with $n>2$.

V. CONCLUSIONS

We have studied the optical properties of high-quality V-groove $GaAs/Al_{0.3}Ga_{0.7}As$ QWRs with three different thicknesses of the GaAs layer. The systematic investigation of PL and PLE spectra as a function of the wire size combined with model calculations has allowed us to study in detail the effect of two-dimensional quantum confinement on valence-band mixing and polarization anisotropy. We have shown that the polarization anisotropy of PL spectra critically depends on localization effects and cannot be related to any polarization analysis based on extended states. The influence of exciton localization and surface corrugation on PLE spectra has also been clarified; the observed large polarization anisotropy has been unambiguously related to the one-dimensional character of our QWRs. Comparison of the experimental results obtained for all three QWR samples with theoretical predictions is clearly compatible with the strong suppression of the 1D band-edge singularity in PLE spectra. We are currently extending our model to include excitonic effects in order to quantify the contribution of interband Coulomb coupling to PLE spectra.

ACKNOWLEDGMENTS

We wish to thank P. Ils and U. Marti for preparing the submicrometer gratings, and G. Biasiol for his contribution to the OMCVD growth of the samples. This work was supported in part by the Fonds National Suisse de la Recherche Scientifique.

[1] See, e.g., W. Jaskólski, Phys. Rep. **271**, 1 (1996); *Proceedings of the 4th International Conference on Optics of Excitons in Confined Systems, Cortona*, edited by F. Bassani, G. C. La Rocca, and A. Quattropani (Nuovo Cimento D **17**, No. 11-12, 1995).
[2] T. Ogawa and T. Takagahara, Phys. Rev. B **44**, 8138 (1991); S. Glutsch and F. Bechstedt, *ibid.* **47**, 4315 (1993).
[3] F. Rossi and E. Molinari, Phys. Rev. Lett. **76**, 3642 (1996).
[4] U. Bockelmann and G. Bastard, Europhys. Lett. **15**, 215 (1991); Phys. Rev. B **45**, 1688 (1992).
[5] D. S. Citrin and Yia-Chung Chang, Phys. Rev. B **43**, 11 703 (1991); P. C. Sercel and K. J. Vahala, *ibid.* **44**, 5681 (1991); C. R. McIntyre and L. J. Sham, *ibid.* **45**, 9443 (1992).
[6] F. Vouilloz, D. Y. Oberli, M.-A. Dupertuis, A. Gustafsson, F. Reinhardt, and E. Kapon, Phys. Rev. Lett. **78**, 1580 (1997); D. Y. Oberli, F. Vouilloz, M.-A. Dupertuis, C. Fall, and E. Kapon, Nuovo Cimento D **17**, 1641 (1995).
[7] E. Kapon, D. M. Hwang, and R. Bhat, Phys. Rev. Lett. **63**, 430 (1989).
[8] D. Gershoni, J. S. Weiner, S. N. G. Chu, G. A. Baraff, J. M. Vandenberg, L. N. Pfeiffer, K. West, R. A. Logan, and T. Tanbun-Ek, Phys. Rev. Lett. **65**, 1631 (1990).
[9] R. Cingolani, M. Lepore, R. Tommasi, I. M. Catalano, H. Lage, D. Heitmann, K. Ploog, A. Shimizu, H. Sakaki, and T. Ogawa, Phys. Rev. Lett. **69**, 1276 (1992).
[10] R. Rinaldi, M. Ferrara, R. Cingolani, U. Marti, D. Martin, F. Morier-Genoud, P. Ruterana, and F. K. Reinhart, Phys. Rev. B **50**, 11 795 (1994).
[11] G. E. W. Bauer and H. Sakaki, Surf. Sci. **267**, 442 (1992).
[12] K. Kash, J. M. Worlock, A. S. Gozdz, B. P. Van der Gaag, J. P. Harbison, P. S. D. Lin, and L. T. Florez, Surf. Sci. **229**, 245 (1990).
[13] A. C. Chen, A. M. Moy, P. J. Pearah, K. C. Hsieh, and K. Y. Cheng, Appl. Phys. Lett. **62**, 1359 (1993).
[14] U. Bockelmann, Europhys. Lett. **16**, 601 (1991).
[15] Y. Kajikawa, Phys. Rev. B **47**, 3649 (1993), and references therein.
[16] G. E. W. Bauer and H. Sakaki, Phys. Rev. B **44**, 5562 (1991).
[17] M. Kohl, D. Heitmann, P. Grambow, and K. Ploog, Phys. Rev. Lett. **63**, 2124 (1989).
[18] H. Lage, D. Heitmann, R. Cingolani, P. Grambow, and K. Ploog, Phys. Rev. B **44**, 6550 (1991).
[19] L. Birotheau, A. Izrael, J. Y. Mauzin, R. Azoulay, V. Thierry-Meig, and F. R. Ladan, Appl. Phys. Lett. **61**, 3023 (1992).
[20] J. Bloch, U. Bockelmann, and F. Laruelle, Europhys. Lett. **28**, 501 (1994).
[21] G. Goldoni, F. Rossi, E. Molinari, A. Fasolino, R. Rinaldi, and R. Cingolani, Appl. Phys. Lett. **69**, 2965 (1996); G. Goldoni, F. Rossi, E. Molinari, and A. Fasolino, Phys. Rev. B **55**, 7110 (1997).
[22] H. Akiyama, T. Someya, and H. Sakaki, Phys. Rev. B **53**, R4229 (1996).
[23] A. Gustafsson, F. Reinhardt, G. Biasiol, and E. Kapon, Appl. Phys. Lett. **67**, 3673 (1995).
[24] P. Ils, Ch. Gréus, A. Forchel, V. D. Kulakovskii, N. A. Gippius, and S. G. Tikhodeev, Phys. Rev. B **51**, 4272 (1995).
[25] E. Ribeiro, F. Cerdeira, and A. Cantarero, Phys. Rev. B **51**, 7890 (1995).
[26] G. Biasiol, F. Reinhardt, A. Gustafsson, E. Martinet, and E. Kapon, Appl. Phys. Lett. **69**, 2710 (1996).
[27] J. Christen, E. Kapon, E. Colas, D. M. Hwang, L. M. Schiavone, M. Grundmann, and D. Bimberg, Surf. Sci. **267**, 257 (1992); S. Haacke, M. Hartig, D. Y. Oberli, B. Deveaud, E. Kapon, U. Marti, and F. K. Reinhart, Solid-State Electron. **40**, 299 (1996).
[28] L. Samuelson, A. Gustafsson, D. Hessman, J. Lindahl, L. Montelius, A. Petersson, and M.-E. Pistol, Phys. Status Solidi A **152**, 269 (1995).
[29] C. Kiener, L. Rota, A. C. Maciel, J. M. Freyland, and J. F. Ryan, Appl. Phys. Lett. **68**, 2061 (1996).
[30] L. W. Molenkamp, R. Eppenga, G. W. 't Hooft, P. Dawson, C. T. Foxon, and K. J. Moore, Phys. Rev. B **38**, 4314 (19988).
[31] G. Bastard, *Wave Mechanics Applied to Semiconductor Heterostructures* (Les Editions de Physique, Les Ulis, 1988).
[32] J. M. Luttinger and W. Kohn, Phys. Rev. **97**, 869 (1955).
[33] J. M. Luttinger, Phys. Rev. **102**, 1030 (1956).
[34] Carriers were photoexcited into the wire by using energy-selective excitation.
[35] J. E. Fouquet, IEEE J. Quantum Electron. **QE-22**, 1799 (1986).
[36] F. Reinhardt, B. Dwir, and E. Kapon, Appl. Phys. Lett. **68**, 3168 (1996).
[37] E. Kapon, K. Kash, E. M. Clausen Jr., D. M. Hwang, and E. Colas, Appl. Phys. Lett. **60**, 477 (1992).
[38] R. C. Miller and R. Bhat, J. Appl. Phys. **64**, 3647 (1988).
[39] D. Gammon, E. S. Snow, B. V. Shanabrook, D. S. Katzer, and D. Park, Phys. Rev. Lett. **76**, 3005 (1996).
[40] K. Brunner, G. Abstreiter, G. Böhm, G. Tränkle, and G. Weimann, Appl. Phys. Lett. **64**, 3320 (1994).
[41] D. Gammon, E. S. Snow, and D. S. Katzer, Appl. Phys. Lett. **67**, 2391 (1995).
[42] U. Jahn, S. H. Kwok, M. Ramsteiner, R. Hey, H. T. Grahn, and E. Runge, Phys. Rev. B **54**, 2733 (1996).
[43] M. Gurioli, A. Vinattieri, J. Martinez-Pastor, and M. Colocci, Phys. Rev. B **50**, 11 817 (1994).
[44] M. Kohl, D. Heitmann, P. Grambow, and K. Ploog, Phys. Rev. B **42**, 2941 (1990).
[45] M. Kohl, D. Heitmann, P. Grambow, and K. Ploog, Phys. Rev. B **37**, 10 927 (1988).
[46] P. C. Sercel and K. J. Vahala, Phys. Rev. B **44**, 5681 (1991).
[47] R. C. Miller and D. A Kleinman, J. Lumin. **30**, 520 (1985), and references therein.
[48] G. Lampel, Phys. Rev. Lett. **20**, 491 (1968).
[49] A. Twardowski and C. Hermann, Phys. Rev. B **35**, 8144 (1987).
[50] C. Weisbuch, R. C. Miller, R. Dingle, A. C. Gossard, and W. Wiegmann, Solid State Commun. **37**, 219 (1981).
[51] R. Winkler, Phys. Rev. B **51**, 14 395 (1995).
[52] F. Rossi and E. Molinari, Phys. Rev. B **53**, 16 462 (1996).
[53] G. E. W. Bauer and T. Ando, Phys. Rev. B **38**, 6015 (1988).
[54] It should be noted that for clarity in Fig. 3(b) of Ref. 6 (F. Vouilloz *et al.*) only e_n-h_n transitions are indicated at photon energy larger than 1.69 eV.